

Complete transparency with three active-passive-coupled optical resonators

Xiao-Bo Yan,¹ Liu Yang,² and Bing He^{3,*}

¹*School of Physics and Electronic Engineering, Northeast Petroleum University, Daqing, 163318, China*

²*College of Intelligent Systems Science and Engineering,*

Harbin Engineering University, Harbin, 150001, China

³*Center for Quantum Optics and Quantum Information,
Universidad Mayor, Camino La Pirámide 5750, Huechuraba, Chile*

The phenomena of induced transparency, with the typical examples of electromagnetically induced transparency (EIT) in atomic media and coupled optical resonators, have attracted tremendous interest since their discoveries. Due to the limitations of the involved elements, however, near-100% transmissions were reported under highly demanding experimental conditions for atomic and other media. Based on a structure of three linearly coupled optical resonators, an active one carrying a possibly arbitrary optical gain and two passive ones simply with dissipation, we demonstrate that a transmitted light field can become completely transparent through the structure, which displays all properties similar to those of EIT. Manifested by a destructive interference to annihilate the intracavity field in the resonator directly coupled to the input, this complete transparency exists for any feasible power of the transmitted field and all realizable coupling strengths of the dark resonator with the input and the neighboring resonator, as long as the inter-cavity coupling for two other resonators is adjustable over a suitable range. A free control on the transparency window size and output field intensity can be realized by tuning two inter-cavity couplings without modifying the built-in system parameters.

Since its first observation with a three-level atomic medium [1, 2], the phenomenon of EIT has been extensively studied together with the accompanying slow-light effect [3–9]. Due to non-zero decay rates of the involved atomic levels and additional absorption pathways in the presence of hyperfine or Zeeman sublevels, achieving a complete transparency under EIT condition is difficult. So far, near-100% transmissions were reported with very few setups, such as optically dense rare-earth doped crystal [4], atomic vapor excited with circularly polarized laser of multimode [6], and single artificial atoms of superconductor [10]. On the other hand, there exist the EIT-like phenomena in coupled optical resonators known as coupled-resonator-induced transparency (CRIT) [11–20], and they have developed into a prominent research direction [21–23]. Two linearly coupled dissipative resonators display all properties similar to those of three-level atomic EIT. The addition of nonlinear optical elements into optical resonator also leads to various types of induced transparency [23–29]. Especially, cavity optomechanical systems were found to demonstrate optomechanically induced transparency (OMIT) [30–32], which has stimulated tremendous interests in its research [33–42]. To these cavity systems, it is equally challenging to realize a complete transparency, due to the unavoidable dissipation of the involved elements such as optical resonator or mechanical resonator with a finite quality factor.

Here, we present an experimentally feasible approach to realizing the complete transparency with three linearly

coupled resonators [see Fig. 1(a)]. The structure consists of one active resonator with optical gain and two other dissipative ones. A special cavity dark mode with totally vanishing intracavity field in the dissipative resonator directly coupled to the input emerges under certain conditions, and it realizes the 100% transmission at the center of a transparency window. Unlike various schemes relying on field amplification mechanisms [8, 20, 28, 43], the complete intracavity field cancellation is realizable with an arbitrary optical gain in the neighboring resonator, no matter how large the field loss in the dark cavity can be. Contrary to intuition, it is not necessary to have an correspondingly enhanced gain to balance any amount of increased field damping for the dark cavity, as long as the inter-cavity coupling between two other resonators can be adjusted over a suitable range. Different from atomic EIT and many other induced-transparency scenarios such as CRIT and OMIT, this phenomenon is based on a previously unknown destructive interference that is irrespective of the pump field intensity and the coupling strengths of the others to the dark resonator.

For the structure shown in Fig. 1(a), the symbols \hat{a}_i and ω_i stand for the intracavity mode and the resonance frequency of cavity i ($i = 1, 2, 3$), respectively. The pump field transmitted at the frequency ω_p and with the amplitude $\varepsilon_p = \sqrt{P/(\hbar\omega_p)}$ (P is its power) couples to cavity 1. The active resonator, cavity 2, has the net gain rate $\kappa_2 = \kappa_{2,0}/\left(1 + \frac{\langle \hat{a}_2^\dagger \hat{a}_2 \rangle}{I_S}\right) - \gamma_2 > 0$ (I_S is the gain saturation intensity and γ_2 the damping rate of the cavity) and is coupled to two other dissipative ones with their damping rates κ_1 and κ_3 , respectively, at the inter-cavity couplings J_1 and J_2 , which are determined by the

* bing.he@umayor.cl

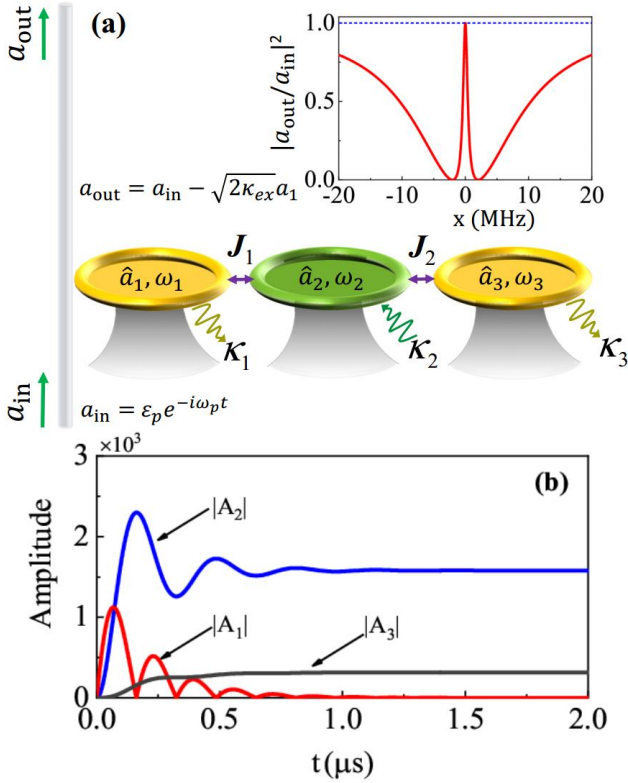


FIG. 1. (a) The schematic structure of three linearly coupled microresonators. Resonator 2 carries a gain medium without showing the external pump used for the field amplification. The actual position of the optical fiber is within the plane of the microresonators. There will be a totally vanishing intracavity field \hat{a}_1 , once resonator 2 and 3 satisfy the condition in Eq. (7). Then, the transmitted field will have the 100% transmission at the center of a narrow frequency window, as shown by the example in the inset, which is obtained with $\kappa_1 = 2\kappa_{ex} = 10$ MHz, $\kappa_2 = 0.2$ MHz, $\kappa_3 = 5$ MHz, and $J_1 = 2$ MHz, and $J_2 = 1$ MHz for three identical microresonators. (b) An example of the evolving intracavity fields after including the optical gain saturation effect. The parameters are $\varepsilon_p = 10^4 \sqrt{\text{MHz}}$ (equivalent to $P = 12.8 \mu\text{W}$ at $\lambda = 1550$ nm), $\kappa_1 = 2\kappa_{ex} = 10$ MHz, $\kappa_{2,0} = 0.2$ MHz, $I_S = 10^8$, $\kappa_3 = 5$ MHz, $J_1 = 20$ MHz, and $J_2 = 1$ MHz. The saturated gain rate after the stabilization is $\kappa_2 = 0.195$ MHz, and the cavity damping rates are chosen to be on the levels of those in some recent experiments [44–46].

distances between the resonators. Hence, similar to those of parity-time (PT) symmetric optical structures [47–52], the effective Hamiltonian of the setup reads as ($\hbar = 1$)

$$\begin{aligned} \hat{H}_{eff} = & \omega_1 \hat{a}_1^\dagger \hat{a}_1 + \omega_2 \hat{a}_2^\dagger \hat{a}_2 + \omega_3 \hat{a}_3^\dagger \hat{a}_3 - J_1 (\hat{a}_1^\dagger \hat{a}_2 + \hat{a}_2^\dagger \hat{a}_1) \\ & - J_2 (\hat{a}_2^\dagger \hat{a}_3 + \hat{a}_3^\dagger \hat{a}_2) + i\sqrt{2\kappa_{ex}}\varepsilon_p (\hat{a}_1^\dagger e^{-i\omega_p t} - \hat{a}_1 e^{i\omega_p t}) \\ & - i\kappa_1 \hat{a}_1^\dagger \hat{a}_1 + i\kappa_2 \hat{a}_2^\dagger \hat{a}_2 - i\kappa_3 \hat{a}_3^\dagger \hat{a}_3, \end{aligned} \quad (1)$$

where the damping rate $\kappa_1 = \kappa_{ex} + \kappa_{in}$ of cavity 1 comes from both external coupling with the pump and its intrinsic loss.

To capture the main physical picture, we will consider

that the gain rate κ_2 quickly saturates to a constant value during the system evolution to a stability, so that the gain rate κ_2 can be treated as a constant. In addition to the previous studies on the relevant effects (see e.g., Refs. [53–57]), the properties of the gain saturation with a real-time $\kappa_2(t)$ in the current scenario, together with the associate gain noise effect [58, 59] which can be neglected in experiments [60], are discussed in Appendix A. Then the effective Hamiltonian in Eq. (1) leads to the following dynamical equation of the operator mean values $a_i(t) = \langle \hat{a}_i(t) \rangle$:

$$\dot{\vec{v}} = \mathbf{M} \vec{v} + \vec{v}_{in} \quad (2)$$

with $\vec{v} = (a_1, a_2, a_3)^T$, $\vec{v}_{in} = (\sqrt{2\kappa_{ex}}\varepsilon_p e^{-i\omega_p t}, 0, 0)^T$, and

$$\mathbf{M} = \begin{pmatrix} -\kappa_1 - i\omega_1 & iJ_1 & 0 \\ iJ_1 & \kappa_2 - i\omega_2 & iJ_2 \\ 0 & iJ_2 & -\kappa_3 - i\omega_3 \end{pmatrix}. \quad (3)$$

In a stable regime (the real parts of all eigenvalues of \mathbf{M} are not positive), the solution to Eq. (2) takes the form $a_k = A_k e^{-i\omega_p t}$ ($k = 1, 2, 3$). Substituting this form into Eq. (2), we obtain the exact solution in the stability:

$$\begin{aligned} A_1 &= \frac{\sqrt{2\kappa_{ex}}\varepsilon_p [J_2^2 - (\kappa_2 + i\Delta_2)(\kappa_3 - i\Delta_3)]}{\eta + [J_1^2 - (\kappa_1 - i\Delta_1)(\kappa_2 + i\Delta_2)](\kappa_3 - i\Delta_3)} \\ A_2 &= \frac{\sqrt{2\kappa_{ex}}\varepsilon_p J_1 (\Delta_3 + i\kappa_3)}{\eta + [J_1^2 - (\kappa_1 - i\Delta_1)(\kappa_2 + i\Delta_2)](\kappa_3 - i\Delta_3)} \\ A_3 &= \frac{-\sqrt{2\kappa_{ex}}\varepsilon_p J_1 J_2}{\eta + [J_1^2 - (\kappa_1 - i\Delta_1)(\kappa_2 + i\Delta_2)](\kappa_3 - i\Delta_3)}, \end{aligned} \quad (4)$$

with $\Delta_i = \omega_p - \omega_i$ ($i = 1, 2, 3$) and $\eta = J_2^2(\kappa_1 - i\Delta_1)$. It can be seen from Eq. (4) that A_2 and A_3 cannot be zero because J_1 , J_2 and κ_3 are non-zero, but A_1 can be zero under certain conditions. These conditions are crucial for achieving a complete transparency. In order to obtain the conditions, we rewrite A_1 in the form of continued fraction:

$$A_1 = \frac{\sqrt{2\kappa_{ex}}\varepsilon_p}{\kappa_1 - i\Delta_1 - \frac{J_1^2}{\kappa_2 + i\Delta_2 - \frac{J_2^2}{\kappa_3 - i\Delta_3}}}. \quad (5)$$

Such continued fraction form can provide a deeper insight into the physical mechanism and helps to conveniently find the complete transparency conditions for the structures of more than three resonators (see Appendix B). The properties of a transmitted light field is determined by the induced A_1 , with the real and imaginary part of the correspondingly defined susceptibility $\varepsilon_T = \sqrt{2\kappa_{ex}}A_1/\varepsilon_p$ (reformulated from a similar definition [30] according to our form of dynamical equation) respectively describing the absorptive and dispersive behavior of a single-frequency input to the structure.

Making the denominator of one subfraction in Eq. (5) vanish, i.e.,

$$\kappa_2 + i\Delta_2 - \frac{J_2^2}{\kappa_3 - i\Delta_3} = 0, \quad (6)$$

will lead to a complete transparency. Under this condition, one has $a_1 = 0$, and the input-output relation in Fig. 1(a) indicates the exactly same output a_{out} as the input $a_{in} = \varepsilon_p e^{-i\omega_p t}$. Since both real and imaginary parts of Eq. (6) should be zero, it follows that

$$\begin{aligned} J_2 &= \sqrt{\frac{\kappa_2 \kappa_3 [(\omega_2 - \omega_3)^2 + (\kappa_2 - \kappa_3)^2]}{(\kappa_2 - \kappa_3)^2}} \\ \omega_p &= \frac{\omega_3 \kappa_2 - \omega_2 \kappa_3}{\kappa_2 - \kappa_3}. \end{aligned} \quad (7)$$

Now we consider three resonators with the same resonance frequency $\omega_1 = \omega_2 = \omega_3 = \omega_0$, so that Eq. (7) can be simplified to

$$\begin{aligned} J_2 &= \sqrt{\kappa_2 \kappa_3} \\ \omega_p &= \omega_0, \end{aligned} \quad (8)$$

and the susceptibility becomes

$$\varepsilon_T = \frac{2\kappa_{ex}}{\kappa_1 - ix - \frac{J_1^2}{\kappa_2 + ix - \frac{\kappa_2 \kappa_3}{\kappa_3 - ix}}}, \quad (9)$$

where $x = \omega_p - \omega_0$. In comparison, the susceptibility of two coupled passive resonators [18, 22] takes the form $\varepsilon_T = 2\kappa_{ex}/[\gamma_1 - ix + J^2/(\gamma_2 - ix)]$, with the corresponding definitions for the coupling and damping rates. The denominator $\gamma_2 - ix$ of its subfraction cannot be zero, due to the second cavity's damping rate $\gamma_2 \neq 0$ in reality.

The solution of the steady intracavity fields,

$$(A_1, A_2, A_3)^T = \sqrt{2\kappa_{ex}}\varepsilon_p \left(0, \frac{i}{J_1}, -\sqrt{\frac{\kappa_2}{\kappa_3}} \frac{1}{J_1} \right)^T, \quad (10)$$

under the conditions of complete transparency in Eq. (8), can be proved to be the zero eigenstate of the effective Hamiltonian in Eq. (1) with $\kappa_2 = \text{constant}$; see Appendix C. Similar to the definition for the networks of linearly coupled bosonic modes [61], the mode \hat{a}_1 with $A_1 = 0$, which is decoupled from all possible excitations of \hat{a}_2 and \hat{a}_3 , is regarded as a cavity dark mode. Different from those formed by atom-photon interactions [62–64] and optomechanical interaction [65, 66], this cavity dark mode is simply created by the linear couplings between the cavities, together with an optical gain in one of them. In this vacuum state $|0\rangle$ of cavity 1, the pump action $\hat{H}_1 = i\sqrt{2\kappa_{ex}}\varepsilon_p(\hat{a}_1^\dagger - \hat{a}_1)$ and the coupling action $\hat{H}_2 = -J_1(A_2\hat{a}_1^\dagger + A_2^*\hat{a}_1)$ from cavity 2 could affect its

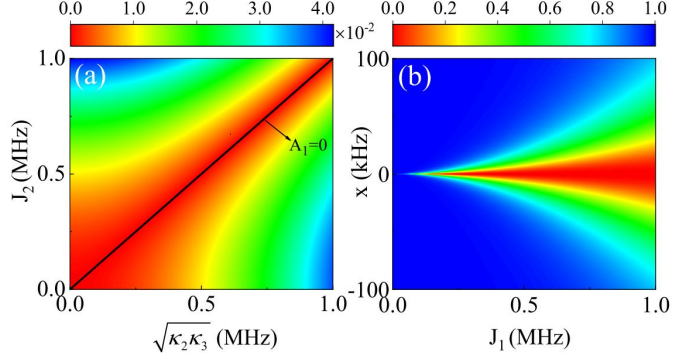


FIG. 2. (a) The distribution of the absolute susceptibility, $|\varepsilon_T| = \sqrt{2\kappa_{ex}}|A_1|/\varepsilon_p$, at $x = 0$, with respect to two parameters $\sqrt{\kappa_2 \kappa_3}$ and J_2 . Here, we fix the rest parameters at $\kappa_1 = 2\kappa_{ex} = 20$ MHz, $\kappa_3 = 5$ MHz, and $J_1 = 10$ MHz. The calculation is based on Eq. (5) but with three identical resonance frequencies. (b) The distribution of $\text{Re}(\varepsilon_T)$ with respect to x and J_1 . Here, the rest of the parameters are set to be $\kappa_1 = 2\kappa_{ex} = 20$ MHz, $\kappa_2 = 0.05$ MHz, $\kappa_3 = 20$ MHz, and $J_2 = 1$ MHz. The calculation is based on Eq. (9).

photon number (see Appendix C). However, one has the exact cancellation

$$\begin{aligned} \langle 1 | \hat{H}_1 + \hat{H}_2 | 0 \rangle &= \langle 1 | i\sqrt{2\kappa_{ex}}\varepsilon_p \hat{a}_1^\dagger - J_1 A_2 \hat{a}_1^\dagger | 0 \rangle \\ &= 0, \end{aligned} \quad (11)$$

with $A_2 = i\sqrt{2\kappa_{ex}}\varepsilon_p/J_1$ in Eq. (10), indicating an absolutely forbidden transition to the excited states of cavity 1. This perfect cancellation exists for all possible values of the directly involved system parameters (J_1 and $\sqrt{2\kappa_{ex}}\varepsilon_p$), in contrast to the destructive interference mechanisms in the previously known scenarios of induced transparency. Tuning the coupling strength J_2 (with the examples on microspheres [15] and microtoroid resonators [67]) so that the system goes close to the diagonal line in Fig. 2(a), one will obtain an approximate dark mode in the red-colored region. Varying the other coupling J_1 will modify the distribution of the approximate dark mode with respect to the detuning x , as shown in Fig. 2(b). It is seen from the continued fraction form in Eq. (5) that no matter how small J_1 is, there exist the approximate dark modes in the neighborhood of the parameter submanifolds determined by Eq. (6).

Once the mode \hat{a}_1 is tuned into a dark mode, the fields in cavity 2 and 3 will exchange the photons with each other in a self-sustained way, i.e., their field losses happen to be compensated by the optical gain, having their photon numbers at the fixed ratio $\langle \hat{a}_2^\dagger \hat{a}_2 \rangle / \langle \hat{a}_3^\dagger \hat{a}_3 \rangle = \kappa_3 / \kappa_2$ without any supply from the pump field. This counter-intuitive phenomenon occurs with any gain rate κ_2 , as long as the coupling J_2 can be correspondingly adjusted according to Eq. (8). At the limit $\kappa_2 \ll \kappa_3$ another resonator, cavity 3, will tend to a dark one as well.

The most important features of the structure are reflected in the absorptive curve of $\text{Re}(\varepsilon_T)$ and the disper-

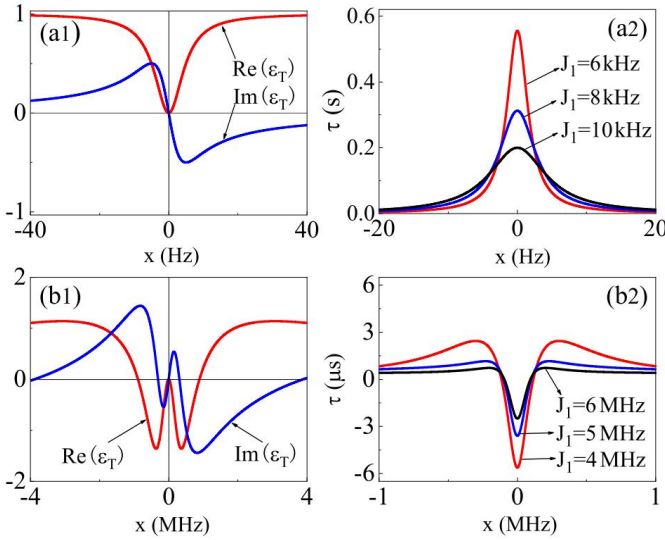


FIG. 3. (a1)-(a2) The examples of $\text{Re}(\varepsilon_T)$ and $\text{Im}(\varepsilon_T)$, as well as the time delays of the transmitted fields, in the regime of $\kappa_2 < \kappa_3$. We use $\kappa_1 = 2\kappa_{\text{ex}} = 20 \text{ MHz}$, $\kappa_2 = 0.01 \text{ MHz}$, $\kappa_3 = 20 \text{ MHz}$, $J_1 = 0.01 \text{ MHz}$ in (a), and $J_2 = \sqrt{\kappa_2\kappa_3}$, so that the transparency window size is in the order of Hz and the time delays approach the order of second. (b1)-(b2) The other examples in the regime of $\kappa_2 > \kappa_3$. The system parameters are set to be $\kappa_1 = 2\kappa_{\text{ex}} = 10 \text{ MHz}$, $\kappa_2 = 1 \text{ MHz}$, $\kappa_3 = 0.1 \text{ MHz}$, and $J_2 = \sqrt{\kappa_2\kappa_3}$. In (b1) we have $J_1 = 4 \text{ MHz}$.

sive curve of $\text{Im}(\varepsilon_T)$. In a situation of $\kappa_2 < \kappa_3$, these curves are exemplified by those in Fig. 3(a1). The size of the transparency window, the full width at half maximum (FWHM) of the curve $\text{Re}(\varepsilon_T)$ around $x = 0$, can be approximated as J_1^2/κ_1 when J_1 is small; cf. the approximate transparency window width $|\Omega|^2/\gamma$ (Ω is the pump Rabi frequency and γ the level decay rate) of three-level atomic EIT. Correspondingly, the slope of the curve of $\text{Im}(\varepsilon_T)$ has the exact form,

$$K = \frac{2\kappa_{\text{ex}}(\kappa_2 - \kappa_3)}{J_1^2\kappa_3} \quad (12)$$

at $x = 0$, happening to be the opposite of the time delay $\tau = \partial \arg(a_{\text{out}}/a_{\text{in}})/\partial \omega_p$ of a transmitted field. In addition to the slow-light effect shown in Fig. 3(a2), the transparency window can be quickly shrunk by reducing the coupling J_1 and enhancing the κ_{ex} to the over-coupling regime, to easily reach the sub-mHz range as the recently proposed nuclear spin induced transparency [68] can realize. For this system satisfying $\kappa_2 < \kappa_3$ and $J_2 = \sqrt{\kappa_2\kappa_3}$, it will keep its dynamical stability over the whole range $0 < J_1 < \infty$ for coupling cavity 1 and 2 (see Appendix D). The above results illustrated by the exactly solved curves of $\text{Re}(\varepsilon_T)$ and $\text{Im}(\varepsilon_T)$, which go through the zero point together under the complete transparency conditions, are irrelevant to the input field intensity, and it is a prominent difference from atomic EIT and OMIT where a transmitted field should be relatively weak.

There will be totally different response to the input, if the prepared gain rate κ_2 surpasses the damping rate κ_3 of a neighboring resonator but keeps the system to be dynamically stable (see Appendix D). Now the curve of $\text{Re}(\varepsilon_T)$ takes the form in Fig. 3(b1), showing a window centered at the minimum amplification. The corresponding curve of $\text{Im}(\varepsilon_T)$ has a slope $K > 0$ at $x = 0$, displaying a fast-light effect with the negatives time delays in Fig. 3(b2).

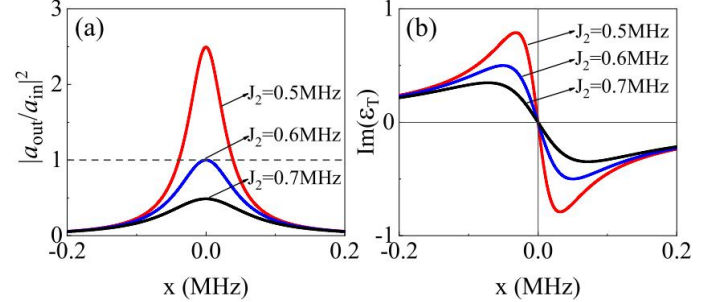


FIG. 4. (a) The comparison between the output/input ratios due to three different couplings J_2 , which are, respective smaller than (the red curve), equal to (the blue curve), and larger than (the black curve) the value $J_{2,c}$ of the 100% transmission at the transparency window center. Represented by these three samples, the output can be continuously amplified or reduced by tuning the coupling J_2 across the point $J_{2,c}$, while the built-in optical gain is unchanged. (b) The corresponding dispersion curves. Here, the fixed system parameter are chosen as $\kappa_1 = 2\kappa_{\text{ex}} = 20 \text{ MHz}$, $\kappa_2 = 0.06 \text{ MHz}$, $\kappa_3 = 6 \text{ MHz}$, and $J_1 = 1 \text{ MHz}$.

Instead of being a limit point that should be asymptotically approached, the 100% transmission rate emerges at a midpoint of tuning the coupling J_2 . As represented by the sample results in Fig. 4(a), tuning the coupling strength from $J_2 > J_{2,c} = \sqrt{\kappa_2\kappa_3}$ to $J_2 < J_{2,c}$ outputs a light field continuously varying from the smaller than the 100% transmission to the larger than the 100% transmission at the transparency window center. The dispersion property demonstrating the slow-light effect is still preserved in the regimes deviating from the complete intracavity field cancellation; see Fig. 4(b). As the distance between cavity 2 and 3 keeps increasing from where cavity 1 is in the vacuum state of completely eliminated intracavity field, which is at $J_{2,c} = 0.6 \text{ MHz}$ for the system described in Fig. 4, more generated photons will go to cavity 1 so that a higher and higher ratio $|a_{\text{out}}/a_{\text{in}}|^2 > 1$ will be achieved until the system loses its dynamical stability at $J_2 = 0.2449 \text{ MHz}$. At a very small coupling J_2 , this system under the condition $J_1 < \sqrt{\kappa_1\kappa_2}$ behaves like two active-passive-coupled resonators in the PT-symmetry broken regime. Although these phenomena of amplifying and reducing the output under a fixed gain rate κ_2 are illustrated with the parameters of high-quality microresonators [44–46], there is no restriction on the qualities of the used optical resonators, since the

conditions on system stability given in Appendix D and a tunable range covering the point $J_{2,c}$ guarantee their occurrence.

In summary, we have presented a scenario of genuinely reducing the susceptibility ε_T of the structure in Fig. 1(a) to zero under the implementable conditions, so that the described phenomenon of complete transparency is totally irrelevant to the input field power. Apart from scanning the input frequency, we only require the tuning of two inter-cavity couplings for seeing the phenomenon: setting one inter-cavity coupling at $J_{2,c} = \sqrt{\kappa_2 \kappa_3}$ and adjusting the other coupling J_1 (possibly together with the external coupling κ_{ex}) for a suitable transparency window size. Rather than being used to cancel the transmission loss, the optical gain plays the role of determining the point $J_{2,c}$ together with the field damping rate in a neighboring resonator, so any nonzero effective gain rate κ_2 can be used in principle. The significance of the scenario lies in two aspects. First, to the research field of induced transparency based on optical resonator [22, 23], it

proves that the ultimate goals of complete transparency and free control on the output/input ratio can be realized without complex designs or particular nonlinear elements. Second, it will non-trivially extend the scope of non-Hermitian photonics based on optical gain. Optical gain in one of two coupled optical resonators provides a realization of PT symmetry [47–52, 60, 69], and the study of the associated phenomenon of exceptional points has been developed into a direction of intensive research [70–72]. Coupling one more resonator will have an even more non-trivial phenomenon involving a special dark mode with its rich properties, and it presents a rare example of something unusual simply built on the common elements like active, passive resonators and their linear couplings.

Acknowledgments—This work was supported by the Program for Young Talents of Basic Research in Universities of Heilongjiang Province (YQJH2024037). L. Y. is supported by National Natural Science Foundation of China (62273115). B. H. is sponsored by ANID Fondecyt Regular (1221250) and thanks Dr. Xiaoshun Jiang for the discussion on the relevant experimental issues.

Appendix

A. Effects of Optical Gain Saturation and Amplification Noise

In non-Hermitian optical models, such as in parity-time (PT) symmetric photonics [48, 52], the systems are often described by the effective non-Hermitian Hamiltonian with a constant optical gain rate. Here, we adopt another approach to the system dynamics from the full quantum view of stochastic Hamiltonian [73], which naturally includes the noise effects such as those from the optical amplification noise [55, 58, 59]. Following the notation in Refs. [55, 59], we write the stochastic Hamiltonian as follows (the definitions for the parameters are the same as those in the main text and $\hbar = 1$):

$$\hat{H} = \omega_1 \hat{a}_1^\dagger \hat{a}_1 + \omega_2 \hat{a}_2^\dagger \hat{a}_2 + \omega_3 \hat{a}_3^\dagger \hat{a}_3 - J_1 (\hat{a}_1^\dagger \hat{a}_2 + \hat{a}_2^\dagger \hat{a}_1) - J_2 (\hat{a}_2^\dagger \hat{a}_3 + \hat{a}_3^\dagger \hat{a}_2) + i\sqrt{2\kappa_{ex}} \varepsilon_p (\hat{a}_1^\dagger e^{-i\omega_p t} - \hat{a}_1 e^{i\omega_p t}) + i\sqrt{2g_2(t)} (\hat{\xi}^\dagger \hat{a}_2^\dagger - \hat{\xi} \hat{a}_2) + i\sqrt{2\kappa_{in}} (\hat{\zeta} \hat{a}_1^\dagger - \hat{\zeta}^\dagger \hat{a}_1) + i\sqrt{2\gamma_2} (\hat{\zeta} \hat{a}_2^\dagger - \hat{\zeta}^\dagger \hat{a}_2) + i\sqrt{2\kappa_3} (\hat{\zeta} \hat{a}_3^\dagger - \hat{\zeta}^\dagger \hat{a}_3), \quad (\text{S-1})$$

where the total losses in cavity 1 give the damping rate $\kappa_1 = \kappa_{in} + \kappa_{ex}$. By applying the Ito's rules for the gain noise operator $\hat{\xi}(t)$ and dissipation noise operator $\hat{\zeta}(t)$, we will obtain the associated dynamical equations of the intracavity field modes:

$$\begin{aligned} \dot{\hat{a}}_1 &= -(\kappa_1 + i\omega_1) \hat{a}_1 + iJ_1 \hat{a}_2 + \sqrt{2\kappa_{ex}} \varepsilon_p e^{-i\omega_p t} + \sqrt{2\kappa_{in}} \hat{\zeta}, \\ \dot{\hat{a}}_2 &= iJ_1 \hat{a}_1 + (g_2(t) - \gamma_2 - i\omega_2) \hat{a}_2 + iJ_2 \hat{a}_3 + \sqrt{2g_2(t)} \hat{\xi}^\dagger + \sqrt{2\gamma_2} \hat{\zeta}, \\ \dot{\hat{a}}_3 &= iJ_2 \hat{a}_2 - (\kappa_3 + i\omega_3) \hat{a}_3 + \sqrt{2\kappa_3} \hat{\zeta}, \end{aligned} \quad (\text{S-2})$$

where the noise operators satisfy the relations $\langle \hat{\xi}(t) \hat{\xi}^\dagger(t') \rangle = \delta(t - t')$ and $\langle \hat{\zeta}^\dagger(t) \hat{\zeta}(t') \rangle = 0$. In some other literature the damping terms take the form $\kappa/2$ while the corresponding noise terms have the factor $\sqrt{\kappa}$. Particularly, we consider the gain saturation effect such that the effective gate rate with time takes the form

$$\kappa_2(t) = \frac{\kappa_{2,0}}{1 + \frac{\langle \hat{a}_2^\dagger \hat{a}_2(t) \rangle}{I_S}} - \gamma_2 = g_2(t) - \gamma_2, \quad (\text{S-3})$$

where $\kappa_{2,0}$ is the initial gain rate when cavity 2 is in the vacuum state, I_S the gain saturation intensity determined by the medium and setup, and γ_2 the damping rate of cavity 2.

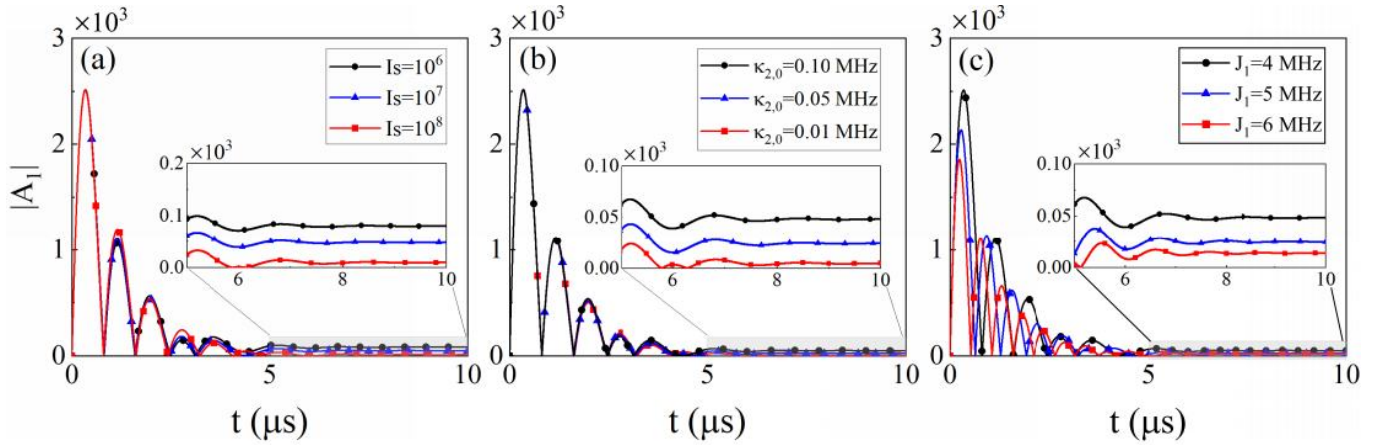


FIG. S-1. (a) Examples of the evolution of the field amplitude $|A_1|$ for different saturation intensities I_S , while the other parameters of the setup are fixed. Here, the initial gain rate is $\kappa_{2,0} = 0.1$ MHz, and $J_1 = 4$ MHz. (b) Examples of the evolution of the field amplitude $|A_1|$ for different initial gain rates $\kappa_{2,0}$, while the other parameters of the setup are fixed. Here, the gain saturation intensity is fixed at $I_S = 10^7$, and $J_1 = 4$ MHz. (c) Examples of the evolution of the field amplitude $|A_1|$ for different inter-cavity couplings J_1 , while the other parameters of the setup are fixed. Here, we have the initial gain rate $\kappa_{2,0} = 0.1$ MHz and the gain saturation intensity $I_S = 10^7$. In all these examples, the fixed system parameters are $\kappa_1 = 2\kappa_{ex} = 2$ MHz and $\kappa_3 = 1$ MHz. The pump field amplitude is fixed at $\varepsilon_p = 10^4 \sqrt{\text{MHz}}$.

In some applications, gain saturation effect leads to optical isolation of coupled optical resonators [53, 56, 60], modifies optomechanical oscillations of hybrid systems [55, 57], and can also influence macroscopic quantum properties of coupled resonators [54]. In our concerned system of three coupled optical resonators, the time-dependent net optical gain rate can affect the intracavity fields. The indicator for the system to evolve to a desired dark mode is whether the field amplitude in the first cavity will finally tend to $|\langle \hat{a}_1 \rangle| = 0$, where $\langle \hat{a}_1 \rangle = A_1 e^{-i\omega_p t}$. We let the system evolve under two conditions: (1) the resonant input for three identical resonance cavity frequencies; (2) $J_2 = \sqrt{\kappa_{2,0}\kappa_3}$ for the chosen system parameters. Without a loss of the described features, we approximate with $\gamma_2 = 0$ in our model calculations because this loss can be compensated by a higher $\kappa_{2,0}$, so that the net gain rate keeps to be $\kappa_2(t) > 0$. For a constant $\kappa_2 = \kappa_{2,0}$, there will emerge an exact $|\langle \hat{a}_1 \rangle| = 0$ under these conditions, as we illustrate in the main text, but this result cannot be guaranteed with a variable $\kappa_2(t)$ in Eq. (S-3). Through the numerical simulations based on Eq. (S-2), we find that three factors affect such processes. The first one of the most obvious is the saturation intensity I_S . Since, the gain rate is the constant $\kappa_{2,0}$ in the limit $I_S \rightarrow \infty$, it is better to have an I_S as higher as possible, as seen from Fig. S-1(a). Due to a lower I_S , the system will evolve to a state obviously deviating from $|\langle \hat{a}_1 \rangle| = 0$. However, this defect can be alleviated by the two other factors that are relevant to the dynamical evolution of the system. In Fig. S-1(b), we fix the gain saturation intensity I_S together with other parameter, but the initial rate $\kappa_{2,0}$ can be varied. A smaller $\kappa_{2,0}$ is beneficial to realizing a state close to the dark mode with $|\langle \hat{a}_1 \rangle| = 0$. Increasing the inter-cavity coupling J_1 between cavity 1 and cavity 2 can also help the realization of the dark mode; see the comparison in Fig. S-1(c) showing that a larger J_1 makes the system evolve to a more suppressed $|\langle \hat{a}_1 \rangle|$. A better dark mode in approximation can be approached with the suitable parameters. For example, with this set of parameters, $\kappa_{2,0} = 10^{-3}$ MHz, $I_S = 10^8$, $J_1 = 10$ MHz, $\kappa_1 = 2\kappa_{ex} = 2$ MHz, and $\kappa_3 = 1$ MHz, the system under the above-mentioned conditions and a resonantly input field with $\varepsilon_p = 10^4 \sqrt{\text{MHz}}$ will have the finally evolved photon number $\langle \hat{a}_1^\dagger \hat{a}_1 \rangle = 7.69 \times 10^{-6}$ in cavity 1.

An interesting point is that the exact dark mode under arbitrary gain saturation can be also realized by adjusting the coupling J_2 . With the computation platforms such as Wolfram Mathematica, we can obtain the steady solution to Eq. (S-2) (after setting the left hand sides of the mean-field version of the equations to be zero) in a highly complex form of continued fraction. The coupling strength J_2 at the point of $|\langle \hat{a}_1 \rangle| = 0$ can be thus numerically found. For example, given a setup with $\kappa_{2,0} = 0.01$ MHz, $I_S = 10^8$, $J_1 = 10$ MHz, $\kappa_3 = 1$ MHz, and $\kappa_1 = 2\kappa_{ex} = 2$ MHz, the coupling rate J_2 between cavity 2 and 3 is numerically found at $J_2 = 0.099$ MHz to achieve the exact $|\langle \hat{a}_1 \rangle| = 0$ under a resonantly input field with $\varepsilon_p = 10^4 \sqrt{\text{MHz}}$. This coupling strength is not far away from the value $J_2 = \sqrt{\kappa_{2,0}\kappa_3}$.

The optical amplification noise is negligible in the realistic situations, though the similar noise demonstrates significance effect in some aspects of PT-symmetric quantum optics (such as quantum Fisher information [74]). It is easy to see that after the system stabilizes, the gain noise term in Eq. (S-2) acts like an independent random drive aside from the coherent drive of the input, generating the extra photons. This amount of extra photons can be accurately

calculated in a stabilized state described by the linear differential equations of the coupled modes. Even for a real-time process due to $\kappa_2(t)$, the evolving photon number due to the optical gain noise can be also calculated with a method used for simulating the dynamical processes of optomechanical cooling [75]. Here we provide an evaluation of the noise contribution with the example in Fig. 1(b) of the main text, in which the extra photons induced by the gain noise to cavity 1 is found to have the number

$$\langle \hat{a}_1^\dagger \hat{a}_1 \rangle_n = \left| C_{1,2} \frac{g_{2,s}}{\lambda_1} \right|^2 = \left| (0.707 - 0.186i) \frac{5.195 \times 10^6}{1.997 \times 10^7} \right|^2 = 3.6 \times 10^{-2},$$

where $C_{1,2}$ is the (1,2)-th element of the rotation matrix for diagonalizing the matrix \mathbf{M} defined in Eq. (3) of the main text (in a reference frame at the pump frequency), $g_{2,s} = \kappa_{2,s} + \gamma_2$ the gain rate after its saturation (the three resonators are assumed to have the same damping rate so that $\gamma_2 = 5$ MHz), and λ_1 the first eigenvalue of the matrix \mathbf{M} . An alternative way for verifying the insignificance of the noise effect is to see on which power level the contribution of the pump drive term $\sqrt{2\kappa_{ex}\varepsilon_p}e^{-i\omega_p t}$ becomes comparable to that of the noise term $\sqrt{2g_2}\hat{\xi}^\dagger$, i.e. the pump power corresponding to $\varepsilon_p = 1 \sqrt{\text{Hz}}$ in Eq. (S-2). For the pump laser in the bandwidth of $\lambda = 1550$ nm, this power is approximately 1.28×10^{-19} Watt, much lower than that of any feasible input. Experimentally the gain noise contribution is not observable even with a gain rate on the order of GHz [60].

B. Induced Transparency with Different Structures

Without loss of generality, we here consider the resonators with the same resonance frequency ω_0 , which are coupled one after another to form a string. The induced transparency phenomenon starts from two coupled passive resonators with their damping rates κ_1 and κ_2 , respectively. From the corresponding dynamics, one finds the steady intracavity field amplitude in cavity 1 as (the notation is consistent with our form of the dynamical equations in the main text):

$$A_1 = \frac{\sqrt{2\kappa_{ex}\varepsilon_p}}{\kappa_1 - ix + \frac{J_1^2}{\kappa_2 - ix}}, \quad (\text{S-4})$$

where $x = \omega_p - \omega_0$. In terms of the continued fraction, this form exactly corresponds to that of the excited level population in a three-level atomic medium for atomic EIT [22], and leads to the transmission rate $T = C^2/(C+1)^2$ at the center of the transparency window, where the cooperativity parameter is given as $C = J_1^2/(\kappa_1\kappa_2)$ (reformulated according to our form of dynamical equations). Like many other types of induced transparency due to mode coupling, its level of transparency continuously improves with the increased inter-cavity coupling J_1 , analogous to the EIT of three-level atomic medium where the Rabi frequency of a much stronger coupling field plays the same role as that of J_1 here, but it can never reach a perfect intracavity field cancellation to $A_1 = 0$, due to the fact $\kappa_1, \kappa_2 \neq 0$. If the second resonator is replaced by an active one with a constant effective gain rate κ_2 , like in PT symmetric photonics [48, 52], the concerned intracavity field amplitude will become

$$A_1 = \frac{\sqrt{2\kappa_{ex}\varepsilon_p}}{\kappa_1 - ix + \frac{J_1^2}{-\kappa_2 - ix}}, \quad (\text{S-5})$$

where the parameter κ_2 changes the sign. In this case, there only exists one trivial possibility of complete transparency at $x = 0$, when the gain rate g_2 of the second resonator gets equal to its intrinsic damping rate γ_2 such that $\kappa_2 = g_2 - \gamma_2 = 0$.

The next step is to couple one more resonator to the above-mentioned structures with the coupling strength J_2 . If all of them are passive ones, we will have the following generalization,

$$A_1 = \frac{\sqrt{2\kappa_{ex}\varepsilon_p}}{\kappa_1 - ix + \frac{J_1^2}{\kappa_2 - ix + \frac{J_2^2}{\kappa_3 - ix}}}, \quad (\text{S-6})$$

from Eq. (S-4) in terms of the continued fraction. This structure has the similar properties to those of two coupled

passive resonators. However, if cavity 2 is replaced by an active one such that κ_2 changes the sign to $-\kappa_2$, i.e.,

$$A_1 = \frac{\sqrt{2\kappa_{ex}\varepsilon_p}}{\kappa_1 - ix + \frac{J_1^2}{-\kappa_2 - ix + \frac{J_2^2}{\kappa_3 - ix}}}, \quad (\text{S-7})$$

the subfraction below the factor J_1^2 in the above expression can totally vanish under the conditions $J_2 = \sqrt{\kappa_2\kappa_3}$ and $x = 0$. It realizes a special dark mode with $A_1 = 0$, which will fundamentally advance instead of quantitatively improving the induced transparency. In contrast to the structures of coupled passive resonators, moreover, the induced transparency with the 100% transmission exists irrespective of the coupling strength J_1 to the first resonator.

Successively one can add one more passive resonator to this string of three coupled resonators, with the dynamical matrix in Eq. (3) of the main text being generalized to

$$\mathbf{M} = \begin{pmatrix} -\kappa_1 - i\omega_0 & iJ_1 & 0 & 0 \\ iJ_1 & \kappa_2 - i\omega_0 & iJ_2 & 0 \\ 0 & iJ_2 & -\kappa_3 - i\omega_0 & iJ_3 \\ 0 & 0 & iJ_3 & -\kappa_4 - i\omega_0 \end{pmatrix}. \quad (\text{S-8})$$

Then, the concerned intracavity field amplitude will be generalized to

$$A_1 = \frac{\sqrt{2\kappa_{ex}\varepsilon_p}}{\kappa_1 - ix + \frac{J_1^2}{-\kappa_2 - ix + \frac{J_2^2}{\kappa_3 - ix + \frac{J_3^2}{\kappa_4 - ix}}}}, \quad (\text{S-9})$$

in terms of the corresponding form of a continued fraction. A complete transparency can be thus realized after meeting the conditions,

$$\begin{aligned} J_2 &= \sqrt{\frac{\kappa_2(J_3^2 + \kappa_3\kappa_4)}{\kappa_4}} \\ \omega_p &= \omega_0, \end{aligned} \quad (\text{S-10})$$

such that the subfraction below the factor J_1^2 in Eq. (S-9) vanishes. Hence, the occurrence of a dark mode in cavity 1 is completely determined by the parameters of the rest resonators—the coupling strengths J_2 and J_3 for the two pairs of the other resonators, together with the damping rates κ_3 , κ_4 and gain rate κ_2 of them. Different from the possible field cancellation to $A_1 = 0$ due to two active-passive-coupled resonators, the gain rate κ_2 in this structure can have arbitrary value, as long as it locates on the submanifold determined by Eq. (S-10), which is possible by means of the adjustment of the other parameters. The generalization to even more resonators in a string is straightforward. Even if the structure is further extended beyond a string of coupled resonators, it will be still feasible to have the modified forms of continued fraction, similar to a practice in the atomic EIT involving multiple energy levels [9]. These continued fractions give us the more complex submanifolds, on which the complete transparency through the structures can be realized while the parameter spaces grow to the higher and higher dimensions.

C. Cavity Dark Mode and Effective Hamiltonian

The effective Hamiltonian in Eq. (1) of the main text takes the form,

$$\begin{aligned} \hat{H}_{eff} &= (-\Delta_1 - i\kappa_1)\hat{a}_1^\dagger\hat{a}_1 + (-\Delta_2 + i\kappa_2)\hat{a}_2^\dagger\hat{a}_2 + (-\Delta_3 - i\kappa_3)\hat{a}_3^\dagger\hat{a}_3 - J_1(\hat{a}_1^\dagger\hat{a}_2 + \hat{a}_2^\dagger\hat{a}_1) \\ &\quad - J_2(\hat{a}_2^\dagger\hat{a}_3 + \hat{a}_3^\dagger\hat{a}_2) + i\sqrt{2\kappa_{ex}\varepsilon_p}(\hat{a}_1^\dagger - \hat{a}_1), \end{aligned} \quad (\text{S-11})$$

in the reference frame rotating at the pump frequency ω_p . Like a laser beam successively split by a group of beamsplitters, the cavity field state due to the action of the above Hamiltonian is a product of coherent states

$|\alpha_1, \alpha_2, \alpha_3\rangle = |A_1, A_2, A_3\rangle$, with $\hat{a}_i |A_i\rangle = A_i |A_i\rangle$ for $i = 1, 2, 3$. Under the condition $J_2 = \sqrt{\kappa_2 \kappa_3}$, the evolved intracavity fields are the following:

$$\begin{aligned} A_1 &= 0 \\ A_2 &= \frac{i}{J_1} \times \sqrt{2\kappa_{ex}} \varepsilon_p \\ A_3 &= -\frac{\sqrt{\kappa_2 \kappa_3}}{J_1 \kappa_3} \times \sqrt{2\kappa_{ex}} \varepsilon_p, \end{aligned} \quad (\text{S-12})$$

for three cavities with the same resonance frequency $\omega_1 = \omega_2 = \omega_3 = \omega_0$, which are under the pump of the detuning $x = \omega_p - \omega_0 = 0$. The effective Hamiltonian will be thus reduced to

$$\begin{aligned} \hat{H}_{eff} &= -i\kappa_1 \hat{a}_1^\dagger \hat{a}_1 + i\kappa_2 \hat{a}_2^\dagger \hat{a}_2 - i\kappa_3 \hat{a}_3^\dagger \hat{a}_3 - J_1(\hat{a}_1^\dagger \hat{a}_2 + \hat{a}_2^\dagger \hat{a}_1) \\ &\quad - J_2(\hat{a}_2^\dagger \hat{a}_3 + \hat{a}_3^\dagger \hat{a}_2) + i\sqrt{2\kappa_{ex}} \varepsilon_p (\hat{a}_1^\dagger - \hat{a}_1). \end{aligned} \quad (\text{S-13})$$

When the system is in the state $|0, A_2, A_3\rangle$, where A_2 and A_3 are given in Eq. (S-12), the action of the Hamiltonian in Eq. (S-13) will be

$$\begin{aligned} \hat{H}_{eff} |0, A_2, A_3\rangle &= \left(i\kappa_2 \hat{a}_2^\dagger \hat{a}_2 - i\kappa_3 \hat{a}_3^\dagger \hat{a}_3 - J_1 \hat{a}_1^\dagger \hat{a}_2 - J_2(\hat{a}_2^\dagger \hat{a}_3 + \hat{a}_3^\dagger \hat{a}_2) + i\sqrt{2\kappa_{ex}} \hat{a}_1^\dagger \varepsilon_p \right) |0, A_2, A_3\rangle, \\ &= \underbrace{(-J_1 \hat{a}_1^\dagger \hat{a}_2 + i\sqrt{2\kappa_{ex}} \hat{a}_1^\dagger \varepsilon_p)}_{=0} |0, A_2\rangle + \underbrace{\left(i\kappa_2 \hat{a}_2^\dagger \hat{a}_2 - i\kappa_3 \hat{a}_3^\dagger \hat{a}_3 - J_2(\hat{a}_2^\dagger \hat{a}_3 + \hat{a}_3^\dagger \hat{a}_2) \right)}_{\hat{H}_R} |A_2, A_3\rangle, \end{aligned} \quad (\text{S-14})$$

where we have used

$$(-J_1 \hat{a}_1^\dagger \hat{a}_2 + i\sqrt{2\kappa_{ex}} \hat{a}_1^\dagger \varepsilon_p) |0, A_2\rangle = (-J_1 A_2 + i\sqrt{2\kappa_{ex}} \varepsilon_p) |1, A_2\rangle = 0 \quad (\text{S-15})$$

according to the solution in Eq. (S-12).

The remaining Hamiltonian in Eq. (S-14) can be written as

$$\hat{H}_R = i\kappa_2 \hat{a}_2^\dagger \hat{a}_2 - i\kappa_3 \hat{a}_3^\dagger \hat{a}_3 - J_2(\hat{a}_2^\dagger \hat{a}_3 + \hat{a}_3^\dagger \hat{a}_2) = i\hat{b}^\dagger \hat{d} \quad (\text{S-16})$$

where

$$\begin{aligned} \hat{b} &= -i\sqrt{\kappa_2} \hat{a}_2 - \sqrt{\kappa_3} \hat{a}_3 \\ \hat{d} &= -i\sqrt{\kappa_2} \hat{a}_2 + \sqrt{\kappa_3} \hat{a}_3 \end{aligned} \quad (\text{S-17})$$

Acting the operator \hat{d} on the state $|A_2, A_3\rangle$, we have

$$\hat{d} |A_2, A_3\rangle = (-i\sqrt{\kappa_2} A_2 + \sqrt{\kappa_3} A_3) |A_2, A_3\rangle = 0, \quad (\text{S-18})$$

due to the solution in Eq. (S-12) again. Hence, the state $|0, A_2, A_3\rangle$ is the one with the zero eigenvalue for the Hamiltonian \hat{H}_{eff} , i.e., $\hat{H}_{eff} |0, A_2, A_3\rangle = 0$ for the A_2 and A_3 in Eq. (S-12). We call the operator \hat{d} the dark-state operator and \hat{b} the bright-state operator. They are not orthogonal, i.e., $[b, d^\dagger] \neq 0$, as a characteristic of non-Hermitian optical systems (see, e.g., Supplementary Materials of Ref. [76]).

Confined to the state $|0, A_2\rangle$ of the first two cavities, only the two terms, $-J_1 \hat{a}_1^\dagger \hat{a}_2$ and $i\sqrt{2\kappa_{ex}} \hat{a}_1^\dagger \varepsilon_p$, in Eq. (S-14) can affect the photon number in cavity 1. However, their joint action exactly cancel the contribution of each other according to the solution in Eq. (S-12), implying a perfect destructive interference of the field coupled back from cavity 2 with the input from the pump. Then, we define two Hamiltonians $\hat{H}_1 = i\sqrt{2\kappa_{ex}} \varepsilon_p (\hat{a}_1^\dagger - \hat{a}_1)$ and $\hat{H}_2 = -J_1 (A_2 \hat{a}_1^\dagger + A_2^* \hat{a}_1)$ of the equivalent effects for these two sources of interference. The joint action, $\langle 1 | \hat{H}_1 + \hat{H}_2 | 0 \rangle = 0$, forbids the excitation of cavity 1, when the setup is under the conditions $J_2 = \sqrt{\kappa_2 \kappa_3}$ and $x = 0$. This result is irrespective of the parameters J_1 and $\sqrt{2\kappa_{ex}} \varepsilon_p$ that are directly relevant to the field in cavity 1.

D. Dynamical Stability and Experimental Feasibility

Modeled by Eq. (S-2), the structure driven by the input field stabilizes after the gain saturation, so that Eq. (S-2) will finally reduce to a system of linear differential equations with the constant coefficients. Depending on the chosen

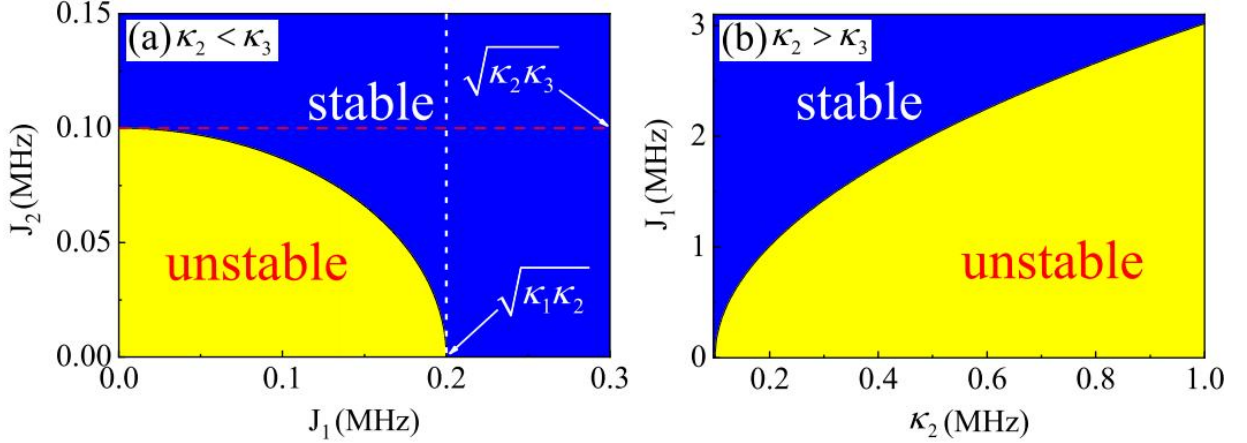


FIG. S-2. (a) One example of the dynamical regimes for the setups with $\kappa_2 < \kappa_3$. The fixed system parameters are chosen as $\kappa_1 = 2\kappa_{ex} = 40$ MHz, $\kappa_2 = 0.001$ MHz, and $\kappa_3 = 10$ MHz. The two coupling strengths J_1 and J_2 are tunable, with their two particular values $\sqrt{\kappa_1\kappa_2} = 0.2$ MHz and $\sqrt{\kappa_2\kappa_3} = 0.1$ MHz for the determination of dynamical stability. (b) The preservation of dynamical stability with the enhanced coupling J_1 , for a setup with $\kappa_2 > \kappa_3$. Here the fixed parameters are set at $\kappa_1 = 2\kappa_{ex} = 10$ MHz, $\kappa_3 = 0.1$ MHz, and the coupling J_2 is variable to be at the values $\sqrt{\kappa_2\kappa_3}$. The horizontal axis starts after $\kappa_2 = 0.1$ MHz, the value of κ_3 .

system parameters, some of the stabilized systems demonstrate the phenomenon of complete transparency, but the others cannot. Here we provide a categorization in the parameter space of the structure.

The above-mentioned feasibility is relevant to the dynamical stability of the system with a constant effective gain rate κ_2 ($I_S \rightarrow \infty$), and it is determined by the eigenvalues of matrix \mathbf{M} defined in Eq. (3) of the main text. The situations of $\kappa_2 < \kappa_3$ have the totally different stable regimes from those of $\kappa_2 > \kappa_3$. To the former, there are the following results for the resonant input fields:

If $J_1 \geq \sqrt{\kappa_1\kappa_2}$, the real parts of the eigenvalues of $\mathbf{M} \leq 0$ for any J_2 ;

If $J_1 < \sqrt{\kappa_1\kappa_2}$, the real parts of the eigenvalues of $\mathbf{M} \leq 0$ when $J_2 > \sqrt{\frac{\kappa_1\kappa_2\kappa_3 - J_1^2\kappa_3}{\kappa_1}}$;

If $J_2 \geq \sqrt{\kappa_2\kappa_3}$, the real parts of the eigenvalues of $\mathbf{M} \leq 0$ for any J_1 ;

If $J_2 < \sqrt{\kappa_2\kappa_3}$, the real parts of the eigenvalues of $\mathbf{M} \leq 0$ when $J_1 > \sqrt{\frac{\kappa_1\kappa_2\kappa_3 - J_2^2\kappa_1}{\kappa_3}}$.

These stable regimes are exemplified in Fig. S-2(a). Here we assume that only the two coupling strengths J_1 and J_2 are tunable by the relative distances between the resonators, with the practical examples for microspheres [15] and microtoroid resonators [67] (the range of tuning J_1 and J_2 of this type of microresonators can be over 1 GHz), while all other system parameters are fixed after the resonators are fabricated. Fig. 4 in the main text presents a process of tuning the coupling J_2 while the value of J_1 is fixed on the left side of the vertical line of $J_1 = \sqrt{\kappa_1\kappa_2}$ in Fig. S-2(a). The coupling J_2 can be continuously tuned downwards across the horizontal line of $J_2 = \sqrt{\kappa_2\kappa_3}$ in Fig. S-2(a), which realizes a complete cancellation of the field in cavity 1, outputting the field from lower than the 100% transmission to higher than the 100% transmission. After the coupling J_2 touches the lower boundary, the system will enter the regime of dynamical instability where the optical gain saturation will play a significant role so that the effective gain rate κ_2 cannot be treated as a constant. On the right side of the vertical line of $J_1 = \sqrt{\kappa_1\kappa_2}$, the output field intensity at the transparency window center will tend to infinitely high as the coupling J_2 is approaching to zero, but the associate transparency window size will gradually vanish at the same time.

If the built-in effective gain rate κ_2 is higher than the damping rate κ_3 in a neighboring resonator, the system will have to reduce the regimes of stability. In this case, the system stability after an increased gain rate κ_2 should be preserved by a correspondingly enhanced inter-cavity coupling J_1 ; see Fig. S-2(b). For the example in Fig. S-2(b),

the coupling J_1 must be increased to 3.017 MHz when the effective gain rate κ_2 reaches 1 MHz (larger than the used $\kappa_3 = 0.1$ MHz). Because the situations of $\kappa_2 > \kappa_3$ are less important, we will not elaborate on the distribution of associated dynamical regimes.

The system dynamics can be as well understood when there is an obvious gain saturation effect. For any possible gain saturation intensity I_S , the gain rate g_2 after saturation (even in the processes of dynamically unstable regimes) will become a constant, so that the system can be nonetheless described by a group of linear differential equations for its coupled intracavity modes. The difference is that the saturated gain rate, $g_{2,s} = \kappa_{2,0} / \left(1 + \frac{\langle \hat{a}_2^\dagger \hat{a}_2 \rangle_s}{I_S} \right)$ ($\langle \hat{a}_2^\dagger \hat{a}_2 \rangle_s$ is the stabilized photon number in the active resonator), will be lowered from the original $\kappa_{2,0}$, and the complete transparency point will be moved to another coupling value $J_2 = \sqrt{(g_{2,s} - \gamma_2) \kappa_3}$ as long as the saturated effective gain rate, $g_{2,s} - \gamma_2$, is still positive. In the dynamically stable regimes determined by the original gain rate $\kappa_{2,0}$ (the effective gain rate κ_2 in Fig. S-2 is replaced by another constant $\kappa_{2,0} - \gamma_2$), the intracavity field intensity or the photon number $\langle \hat{a}_2^\dagger \hat{a}_2 \rangle$ in the active cavity will cause a rather limited shift of the gain rate g_2 from the original $\kappa_{2,0}$, so that the complete transparency can be achieved by a relatively fine tuning of the coupling J_2 to a smaller value; see an example in Appendix A. It is why the complete transparency can be always reached at a coupling J_2 in such dynamically stable regimes, given any feasible gain saturation intensity I_S . One feature is that tuning the coupling J_2 around the point of complete transparency will not lead to a drastic change of the photon number $\langle \hat{a}_2^\dagger \hat{a}_2 \rangle$ in the active resonator. Especially, at the exact point of complete transparency, there is a counter-intuitive photon number $\langle \hat{a}_2^\dagger \hat{a}_2 \rangle_s = 2\kappa_{ex}(\varepsilon_p/J_1)^2$ [from Eq. (S-12)] that is independent of the coupling J_2 and the gain rate, and it provides a mechanism to reduce the gain saturation effect by an enhanced coupling J_1 [exhibited by the results in Fig. S-1(c)]. On the other hand, the optical gain will drop tremendously due to a quick growth of the cavity photon number $\langle \hat{a}_2^\dagger \hat{a}_2 \rangle$ in a dynamically unstable regime, and the stabilized gain rate $g_{2,s}$ will be far away from the original $\kappa_{2,0}$, making it impossible to reach the complete transparency point by tuning the coupling J_2 .

In summary, the phenomenon of complete transparency through the concerned structure of three active-passive-coupled optical resonators should be observed in the dynamically stable regimes determined by its built-in gain rate $\kappa_{2,0}$, which can become smaller with a gain saturation. The system's dynamical stability can be guaranteed if it exists with this original gain rate $\kappa_{2,0}$, because the effective gain will be only lowered after the saturation. With a negligible gain saturation effect, i.e., the field intensity in the active resonator is not high enough to modify the gain rate obviously, the complete transparency point will be located by adjusting the distance between cavity 2 and 3 so that the corresponding coupling goes across the horizontal line $J_2 = \sqrt{\kappa_2 \kappa_3}$ in Fig. S-2(a), and the operation can be performed with any nonzero coupling J_1 between cavity 1 and cavity 2. Even if there exists an obvious gain saturation that shifts the stabilized optical gain rate, the point of complete transparency can still be located by a further tuning of the coupling J_2 to a bit smaller value. Moreover, the gain saturation effect can be well suppressed by enhancing the coupling strength J_1 .

[1] S. E. Harris, J. E. Field, and A. Imamoglu, Nonlinear optical processes using electromagnetically induced transparency, *Phys. Rev. Lett.* 64, 1107 (1990).

[2] K.-J. Boller, A. Imamoglu, and S. E. Harris, Observation of electromagnetically induced transparency, *Phys. Rev. Lett.* 66, 2593 (1991).

[3] M. Fleischhauer, A. Imamoglu, and J. P. Marangos, Electromagnetically induced transparency: Optics in coherent media, *Rev. Mod. Phys.* 77, 633 (2005).

[4] B. S. Ham, P. R. Hemmer, and M. S. Shahriar, Efficient electromagnetically induced transparency in a rare-earth doped crystal, *Opt. Commun.* 144, 227 (1997).

[5] L. V. Hau, S. E. Harris, Z. Dutton, and C. H. Behroozi, Light speed reduction to 17 metres per second in an ultracold atomic gas, *Nature* 397, 594 (1999).

[6] G. Alzetta, S. Gozzini, A. Lucchesini, S. Cartaleva and T. Karaulanov, C. Marinelli, and L. Moi, Complete electromagnetically induced transparency in sodium atoms excited by a multimode dye laser, *Phys. Rev. A* 69, 063815 (2004).

[7] I. Novikova, R. L. Walsworth, and Y. Xiao, Electromagnetically induced transparency-based slow and stored light in warm atoms, *Laser Photon. Rev.* 6, 333 (2012).

[8] D. Wang, C. Liu, C. Xiao, J. Zhang, H. M. M. Alotaibi, B. C. Sanders, L.-G. Wang, and S. Zhu, Strong coherent light amplification with double electromagnetically induced transparency coherences, *Sci. Rep.* 7, 5796 (2017).

[9] R. Finkelstein, S. Bali, O. Firstenberg, and I. Novikova, A practical guide to electromagnetically induced transparency in atomic vapor, *New J. Phys.* 25, 035001 (2023).

[10] A. A. Abdumalikov, Jr., O. Astafiev, A. M. Zagoskin, Yu. A. Pashkin, Y. Nakamura, and J. S. Tsai, Electromagnetically Induced Transparency on a Single Artificial Atom, *Phys. Rev. Lett.* 104, 193601 (2010).

[11] A. Yariv, Y. Xu, R. K. Lee, and A. Scherer, Coupled-resonator optical waveguide: a proposal and analysis, *Opt. Lett.* 24, 711 (1999).

[12] D. D. Smith, H. Chang, K. A. Fuller, A. T. Rosenberger, and R. W. Boyd, Coupled-resonator-induced transparency, *Phys. Rev. A* 69, 063804 (2004).

[13] L. Maleki, A. B. Matsko, A. A. Savchenkov, and V. S. Ilchenko, Tunable delay line with interacting whispering-gallery-mode resonators, *Opt. Lett.* 29, 6 (2004).

[14] Q. Xu, S. Sandhu, M. L. Povinelli, J. Shakya, S. Fan, and M. Lipson, Experimental Realization of an On-Chip All-Optical Analogue to Electromagnetically Induced Transparency, *Phys. Rev. Lett.* 96, 123901 (2006).

[15] K. Totsuka, N. Kobayashi, and M. Tomita, Slow Light in Coupled-Resonator-Induced Transparency, *Phys. Rev. Lett.* 98, 213904 (2007).

[16] Y.-F. Xiao, L. He, J. Zhu, and L. Yang, Electromagnetically induced transparency-like effect in a single polydimethylsiloxane-coated silica microtoroid, *Appl. Phys. Lett.* 94, 231115 (2009).

[17] X. Yang, M. Yu, D.-L. Kwong, and C. W. Wong, All-Optical Analog to Electromagnetically Induced Transparency in Multiple Coupled Photonic Crystal Cavities, *Phys. Rev. Lett.* 102, 173902 (2009).

[18] B. Peng, S. K. Özdemir, W. Chen, F. Nori, and L. Yang, What is and what is not electromagnetically induced transparency in whispering-gallery microcavities, *Nat. Commun.* 5, 5082 (2014).

[19] C. Wang, X. Jiang, W. R. Sweeney, C. W. Hsu, Y. Liu, G. Zhao, B. Peng, M. Zhang, L. Jiang, A. D. Stone, and L. Yang, Induced transparency by interference or polarization, *Proc. Natl. Acad. Sci.* 118, e2012982118 (2021).

[20] D. Sugio, T. Manabe, K. Nakamura, T. Matsumoto, and M. Tomita, Observation of the transition from inverted coupled-resonator-induced transparency to inverted Autler-Townes splitting, *Phys. Rev. A* 107, 013110 (2023).

[21] R. W. Boyd and D. J. Gauthier, Photonics: transparency on an optical chip, *Nature* 441, 701 (2006).

[22] Y.-C. Liu, B.-B. Li, and Y.-F. Xiao, Electromagnetically induced transparency in optical microcavities, *Nanophotonics* 6, 789-811 (2017).

[23] H. Qin, M. Ding, and Y. Yin, Induced Transparency with Optical Cavities, *Adv. Photonics Research* 1, 2000009 (2020).

[24] S. Zhang, D. A. Genov, Y. Wang, M. Liu, and X. Zhang, Plasmon-Induced Transparency in Metamaterials, *Phys. Rev. Lett.* 101, 047401 (2008).

[25] R. Puthumpally-Joseph, M. Sukharev, O. Atabek, and E. Charroux, Dipole-Induced Electromagnetic Transparency, *Phys. Rev. Lett.* 113, 163603 (2014).

[26] C.-H. Dong, Z. Shen, C.-L. Zou, Y.-L. Zhang, W. Fu, and G.-C. Guo, Brillouin-scattering-induced transparency and non-reciprocal light storage, *Nat. Commun.* 6, 6193 (2015).

[27] J. Kim, M. C. Kuzyk, K. Han, H. Wang, and G. Bahl, Non-reciprocal Brillouin scattering induced transparency, *Nature Physics* 11, 275 (2015).

[28] Y. Zheng, J. Yang, Z. Shen, J. Cao, X. Chen, X. Liang, and W. Wan, Optically induced transparency in a microcavity, *Light Sci. Appl.* 5, 16072 (2016).

[29] J. Ma, J. Qin, G. T. Campbell, R. Lecamwasam, K. Sripathy, J. Hope, B. C. Buchler, and P. K. Lam, Photothermally induced transparency, *Sci. Adv.* 6, eaax8256 (2020).

[30] G. S. Agarwal and S. Huang, Electromagnetically induced transparency in mechanical effects of light, *Phys. Rev. A* 81, 041803(R) (2010).

[31] S. Weis, R. Rivière, S. Deléglise, E. Gavartin, O. Arcizet, A. Schliesser, and T. J. Kippenberg, Optomechanically Induced Transparency, *Science* 330, 1520–1523 (2010).

[32] A. H. Safavi-Naeini, T. P. Mayer Alegre, J. Chan, M. Eichenfield, M. Winger, Q. Lin, J. T. Hill, D. E. Chang, and O. Painter, Electromagnetically induced transparency and slow light with optomechanics, *Nature* 472, 69 (2011).

[33] S. Huang and G. S. Agarwal, Electromagnetically induced transparency from two-phonon processes in quadratically coupled membranes, *Phys. Rev. A* 83, 023823 (2011).

[34] D. E. Chang, A. H. Safavi-Naeini, M. Hafezi, and O. Painter, Slowing and stopping light using an optomechanical crystal array, *New J. Phys.* 13, 023003 (2011).

[35] H. Xiong, L.-G. Si, A.-S. Zheng, X. Yang, and Y. Wu, Higher-order sidebands in optomechanically induced transparency, *Phys. Rev. A* 86, 013815 (2012).

[36] M. Karuza, C. Biancofiore, M. Bawaj, C. Molinelli, M. Galassi, R. Natali, P. Tombesi, G. Di Giuseppe, and D. Vitali, Optomechanically induced transparency in a membrane-in-the-middle setup at room temperature, *Phys. Rev. A* 88, 013804 (2013).

[37] A. Kronwald and F. Marquardt, Optomechanically Induced Transparency in the Nonlinear Quantum Regime, *Phys. Rev. Lett.* 111, 133601 (2013).

[38] D. Tarhan, S. Huang, and Ö. E. Müstecaplıoğlu, Superluminal and ultraslow light propagation in optomechanical systems, *Phys. Rev. A* 87, 013824 (2013).

[39] H. Jing, S. K. Özdemir, Z. Geng, J. Zhang, X.-Y. Lü, B. Peng, L. Yang, and F. Nori, Optomechanically-induced transparency in parity-time-symmetric microresonators, *Sci. Rep.* 5, 9663 (2015).

[40] H. Lü, C. Wang, L. Yang, and H. Jing, Optomechanically Induced Transparency at Exceptional Points, *Phys. Rev. Applied* 10, 014006 (2018).

[41] X. B. Yan, Optomechanically induced transparency and gain, *Phys. Rev. A* 101, 043820 (2020).

[42] X. B. Yan, Optomechanically induced ultraslow and ultrafast light, *Phys. E* 131, 114759 (2021).

[43] G. Strangi, A. De Luca, S. Ravaine, M. Ferrie, and R. Bartolino, Gain induced optical transparency in metamaterials, *Appl. Phys. Lett.* 98, 251912 (2011).

[44] X. Li, K. Qi, Y. Wu, X. Wu, M. Hu, Z. Li, Y. He, S. Ding, Z. Xie, H. Zhou, B. He, M. Xiao, and X. Jiang, Generation of 2/3-octave-spanning visible Kerr soliton microcomb, *Adv. Photon.* 7, 056002 (2025).

[45] Q. Shi, J. Tian, S. Ding, Y. Wang, S. Lei, M. Zhang, W. Wan, X. Ji, B. He, M. Xiao, and X. Jiang, On-chip ultrahigh-Q optical microresonators approaching the material absorption limit, *Photonics Res.* 13, 2409 (2025).

[46] X. Li, Y. Xie, S. Ding, M. Zhang, Y. He, B. He, M. Xiao, and X. Jiang, Observation of Kerr soliton microcomb locked with a phonon laser, *Sci. Adv.* 12, eaeb3400 (2026).

[47] A. A. Zyablovsky, A. P. Vinogradov, A. A. Pukhov, A. V. Dorofeenko, and A. A. Lisiansky, PT-symmetry in optics, *Phys.-Usp.* 57, 1063 (2014).

[48] V. V. Konotop, J. Yang, and D. A. Zezyulin, Nonlinear waves in PT-symmetric systems, *Rev. Mod. Phys.* 88, 035002 (2016).

[49] J. Wen, X. Jiang, L. Jiang, and M. Xiao, Parity-time symmetry in optical microcavity systems, *J. Phys. B: At. Mol. Opt. Phys.* 51, 222001 (2018).

[50] S. K. Özdemir, S. Rotter, F. Nori, and L. Yang, Parity-time symmetry and exceptional points in photonics, *Nat. Mater.* 18, 783 (2019).

[51] C. Wang, Z. Fu, W. Mao, J. Qie, A. D. Stone, and L. Yang, Non-Hermitian optics and photonics: from classical to quantum, *Adv. Opt. Photon.* 15, 442-523 (2023).

[52] C. Zhang, M. Kim, Y.-H. Zhang, Y.-P. Wang, D. Trivedi, A. Krasnok, J. Wang, D. Isleifson, R. Roshko, and C.-M. Hu, Gain-Loss Coupled Systems, *APL Quantum* 2, 011501 (2025).

[53] B. He, L. Yang, X. Jiang, and M. Xiao, Transmission Nonreciprocity in a Mutually Coupled Circulating Structure, *Phys. Rev. Lett.* 120, 203904 (2018).

[54] S. Vashahri-Ghamsari, B. He, and M. Xiao, Effects of gain saturation on the quantum properties of light in a non-Hermitian gain-loss coupler, *Phys. Rev. A* 99, 023819 (2019).

[55] Y. Xie, Z. Cao, B. He, and Q. Lin, PT-symmetric phonon laser under gain saturation effect, *Opt. Express* 28, 22580-22593 (2020).

[56] Z. Cao, Y. Xie, B. He, and Q. Lin, Ultra-high optical nonreciprocity with a coupled triple-resonator structure, *New J. Phys.* 23 023010 (2021).

[57] X. Z. Hao, X. Y. Zhang, Y. H. Zhou, W. Li, S. C. Hou, and X. X. Yi, Gain-saturation-induced self-sustained oscillations in non-Hermitian optomechanics, *Phys. Rev. A* 103, 053508 (2021).

[58] G. S. Agarwal and K. Qu, Spontaneous generation of photons in transmission of quantum fields in PT-symmetric optical systems, *Phys. Rev. A* 85, 031802(R) (2012).

[59] S. Vashahri-Ghamsari and B. He, Gain Saturation Modified Quantum Noise Effect on Preparing a Continuous-Variable Entanglement, *Photonics* 9, 620 (2022).

[60] L. Chang, X. Jiang, S. Hua, C. Yang, J. Wen, L. Jiang, G. Li, G. Wang, and M. Xiao, Parity-time symmetry and variable optical isolation in active-passive-coupled microresonators, *Nat. Photon.* 8, 524 (2014).

[61] J. Huang, C. Liu, X.-W. Xu, and J.-Q. Liao, Dark-mode theorems for quantum networks, *arXiv:2312.06274*.

[62] D. H. White, S. Kato, N. Német, S. Parkins, and T. Aoki, Cavity dark mode of distant coupled atom-cavity systems, *Phys. Rev. Lett.* 122, 253603 (2019).

[63] S. Kato, N. Német, K. Senga, S. Mizukami, X. Huang, S. Parkins, and T. Aoki, Observation of dressed states of distant atoms with delocalized photons in coupledcavities quantum electrodynamics, *Nat. Commun.* 10, 1160 (2019).

[64] X. Zhang, Z. Yu, H. Zhang, D. Xiang, and H. Zhang, Cavity dark mode mediated by atom array without atomic scattering loss, *Phys. Rev. Research* 6, L042026 (2024).

[65] C. Dong, V. Fiore, M. C. Kuzyk, and H. Wang, Optomechanical dark mode, *Science* 338, 1609 (2012).

[66] J. T. Hill, A. H. Safavi-Naeini, J. Chan, and O. Painter, Coherent optical wavelength conversion via cavity optomechanics, *Nat. Commun.* 3, 1196 (2012).

[67] C. Yang, X. Jiang, Q. Hua, S. Hua, Y. Chen, J. Ma, and M. Xiao, Realization of controllable photonic molecule based on three ultrahigh-Q microtoroid cavities, *Laser Photon. Rev.* 11, 1600178 (2017).

[68] H.-b. Zhang, Y. Tang, and Y.-C. Liu, Nuclear spin induced transparency, *Phys. Rev. Research* 7, L012069 (2025).

[69] B. Peng, S. K. Özdemir, F. Lei, F. Monifi, M. Gianfreda, G. L. Long, S. Fan, F. Nori, C. M. Bender, and L. Yang, Parity-time-symmetric whispering-gallery microcavities, *Nat. Phys.* 10, 394 (2014).

[70] M. A. Miri and A. Alú, Exceptional points in optics and photonics, *Science* 363, eaar7709 (2019).

[71] J. Wiersig, Review of exceptional point-based sensors, *Photonics Res.* 8, 1457-1467 (2020).

[72] H. Meng, Y. S. Ang, and C. H. Lee, Exceptional points in non-Hermitian systems: Applications and recent developments, *Appl. Phys. Lett.* 124, 060502 (2024).

[73] C. W. Gardiner and P. Zoller, *Quantum Noise*, Springer-Verlag, Berlin Heidelberg, 2000.

[74] W. Wang, Y. Zhai, D. Liu, X. Jiang, S. Vashahri-Ghamsari, and J. Wen, Quadrature-PT symmetry: Classical-to-quantum transition in noise fluctuations, *Quantum Sci. Technol.* 10, 025016 (2025).

[75] B. He, L. Yang, Q. Lin, and M. Xiao, Radiation Pressure Cooling as a Quantum Dynamical Process, *Phys. Rev. Lett.* 118, 233604 (2017).

[76] B. He, L. Yang, and M. Xiao, Dynamical phonon laser in coupled active-passive microresonators, *Phys. Rev. A* 94, 031802(R) (2016).